Marine Structures 80 (2021) 103079

Contents lists available at ScienceDirect

Marine Structures

journal homepage: www.elsevier.com/locate/marstruc

Permanent accumulated rotation of offshore wind turbine monopile due to typhoon-induced cyclic loading

Hongwang Ma [a,*], Zhiyue Lu [a], Yutao Li [a], Chen Chen [a], Jun Yang [b]

[a] School of Naval Architecture, Ocean and Civil Engineering, Shanghai Jiao Tong University, Shanghai, China
[b] Department of Civil Engineering, The University of Hong Kong, Hong Kong, China

ARTICLE INFO

Keywords:
Typhoon
Monopile foundation
Offshore wind turbine
Accumulated rotation

ABSTRACT

In order to study the effect of typhoons on the accumulated deformation of monopile foundations for offshore wind turbines, a series of 1-g laboratory model tests with a geometrical scale of 1:100 were carried out. Through the horizontal static and cyclic loading tests of a stiff pile embedded in a medium dense sand deposit, the relationship between the accumulated rotation of the pile and the number of loading cycles under different loading conditions was obtained. The results show that the final accumulated rotation is mainly caused by the typhoon load series and is not affected by the loading sequence. Based on these results, a method is presented to predict the accumulated rotation of the monopile foundation during its service life, and a case study of a 6 MW wind turbine supported by a monopile at a water depth of 30 m in sand is conducted by using the method. The results show that the permanent accumulated rotation of the monopile throughout the design life is mainly contributed by cyclic loading induced by typhoons and the contribution of cyclic loading with small amplitudes can be ignored.

1. Introduction

Offshore wind power currently plays an important role in renewable energy around the world, especially in European countries such as the United Kingdom, Denmark and Germany [1]. Offshore wind power is also under a rapid development in China, with a newly installed capacity of 1.8 GW in 2018, which made China to take the lead for the first time [1]. As far as the foundation type is concerned, monopiles continue to dominate the operating foundation of the offshore wind turbines worldwide, accounting for 73.5 % of the total market [2]. It has been recognized that monopiles offer a cost-effective solution for wind energy converters installed in water depths of up to 30 m or even 40 m [3].

In most cases, the primary design driver of monopile foundations for offshore wind turbines is permanent deformation rather than ultimate capacity [4–8]. The deformation may exceed the normal operating requirements of the turbine even when the foundation is far below the ultimate capacity [6,7]. Under normal operating conditions, the monopile foundation will be subjected to long-term horizontal loads of small amplitudes caused by winds, waves and currents, resulting in accumulated deformation [8]. When the typhoon emanates, it will bring great wind speed and accompanying huge waves and thereby strong cyclic loads on the monopile foundation in a short time. The consequences can be large lateral deformations and even the overall overturning of the pile, which obviously has a significant impact on the permanent accumulated deformation of the monopile foundation [9,10].

For monopiles under cyclic loading with small amplitudes, there have been many studies and valuable results. For example,

* Corresponding author.
E-mail address: hwma@sjtu.edu.cn (H. Ma).

https://doi.org/10.1016/j.marstruc.2021.103079
Received 26 March 2020; Received in revised form 7 June 2021; Accepted 4 July 2021
Available online 13 August 2021

LeBlanc et al. [8] carried out small-scale model tests under 1-g condition to investigate the lateral deformation of a stiff pile in unsaturated sand with relative densities of 4 % and 38 %, respectively, and presented a method for predicting the accumulated rotation in the service life. Abadie et al. [11] performed small-scale laboratory tests on stiff piles subject to lateral cyclic loading in drained sand. The loading rate effects, hysteretic behavior and pile response caused by long-term single and multi-amplitude cyclic loading were studied. The results have shown that the pile response conforms closely to the extended Masing rules [11], and additional permanent deformation is accumulated under the action of non-symmetric cyclic loads. Sun [6] analyzed the effect of cyclic load amplitude, number of loading cycles and other factors on the accumulated deformation of stiff piles based on the results of cyclic loading model test. It was found that there is a linear relationship between the accumulated deformation of the pile and the number of loading cycles in double logarithmic axes. Ma et al. [7] used a simplified computational model to study the effect of long-term cyclic loads on the performance of offshore wind turbine foundations. The study showed that long-term cyclic loading had a significant impact on the lateral deformation of monopile foundations. Cuéllar [12] performed physical model tests on a reduced scale (1:100) of a pile under cyclic lateral load of up to 5 million loading cycles under 1-g conditions. Two particular phenomena were observed, namely a soil subsidence around the pile and a permanent grain migration towards the pile. It was also found that there are three distinct phases of pile-head displacement during cyclic loading, which can be reasonably approximated by the logarithmic function, linear function and power-law function of the number of cycles, respectively. However, there are few studies on large cyclic loads caused by typhoons. Roesen et al. [13] carried out cyclic loading tests on a model pile in saturated sand with a relative density of 85 %–90 %. It was found that the accumulated deformation of the pile increased with increasing cyclic load amplitude and can be expressed using a power function. Barari et al. [9] conducted a large-scale numerical modeling to predict the accumulated monopile rotation under one-way and transient cyclic lateral loading using a numerical model. The results indicated that fewer loading cycles with higher load levels are the main concerns in the accumulated rotation of the pile than thousands of low-amplitude loading cycles. However, there is a lack of experimental data to validate the numerical prediction. Wang et al. [5] presented a workflow to predict the permanent accumulated rotation of a monopile-supported offshore wind turbine in sand during an extreme storm. The effect of fully nonlinear irregular waves versus the commonly used linear wave theory was included, and the method based on Miner's rule [8] was used to predict cyclically accumulated rotation during the storm. The results showed that extremely large loading cycles generate higher accumulated rotation than thousands of small loading cycles.

In this paper, small-scale model tests under 1-g conditions with the aim to study the effect of typhoons on the accumulated rotation of monopile foundations for offshore wind turbines are presented. By applying large-amplitude cyclic loads in different stages of the loading process, the lateral displacements of the pile were measured and the pile rotation at the mudline were determined. Based on the test data for the relation between pile rotation and the number of loading cycles, a method is proposed to calculate the accumulated rotation taking into account the effect of typhoons, and the method is then applied to a case study.

1.1. Model tests

1.1.1. 1-g scaling laws

A typical monopile for a 5 MW turbine, with external diameter of 7.5 m, embedded depth of 37.5 m and length of 80 m [12] was used as a reference in the study. The outer dimension of the pile was scaled to 1:100. Under the 1-g conditions, a scaling design was performed based on Buckingham's Π-theorem [8,11], leading to the scaling laws for the model tests in Table 1.

1.2. Experimental equipment

The model tests were carried out in a specially designed tank with a length of 1.2 m, a width of 0.8 m and a depth of 0.9 m. A dry sand deposit of 0.85 m was prepared in 5 layers and each layer was compacted to the targeted density. An open-ended hollow PVC pile with an external diameter of 75 mm, a wall thickness of 2.44 mm, and a length of 800 mm was used as the model pile. The elastic modulus of this PVC pile is 3.24 GPa, which was measured by the simply supported beam method [14]. The flexural stiffness of this pile was about four times greater than it should be in accordance with the scaling laws presented in Table 1. Since the ratio of this pile makes it behave as a short stiff pile, the distorting effect caused by this extra flexural rigidity may be negligible [12].

The experiments were conducted using a mixing quartz sand (Fujian sand) [15] under dry conditions, whose grain size distribution

Table 1
Scaling laws for model tests under 1 g conditions [12].

Physical quantity	Scaling law	Dimensions
Length, L	$L_M = L_P/\lambda$	L [m]
Force, F	$F_M = F_P/\lambda^3$	F [N]
Stress, σ	$\sigma_M = \sigma_P/\lambda$	F/L^2 [Pa]
Unit weight, γ	$\gamma_M = \gamma_P$	F/L^3 [N/m3]
Moment, M	$M_M = M_P/\lambda^4$	FL [N m]
Bending stiffness, EI	$(EI)_M = (EI)_P/\lambda^5$	FL^2 [N m2]
Time, t	$t_M = t_P/\lambda^{1/2}$	T [s]
Frequency, f	$f_M = f_P/\lambda^{-1/2}$	1/T [Hz]

is similar to that of Berliner sand used in Ref. [12]. In the tests, the sand density of each case was set at 1.60 g/cm^3 with a relative density of about 58 %. The main properties of the sand were tested according to Ref. [16] (GB/T50123-1999), and are summarized in Table 2.

The rocking of the pile was performed by an electric servo actuator. The actuator had a load capacity of approximately 1000 N, a maximum stroke of 200 mm, and a sinusoidal cyclic load with a frequency of 1 Hz. The actuator was placed on a steel frame, and connected to the concrete floor. The force exerted on the pile head was measured by an embedded tension/compression load cell. Two Linear Variable Differential Transformers (LVDTs) displacement transducers were used to obtain continuous measurements of pile displacements with an accuracy of ±0.03 mm, a range of 0–30 mm, and a non-linearity within ±0.1 %. The displacement transducers and servo actuator were connected to the simultaneous data acquisition devices.

1.3. Loading and measuring point arrangement

Fig. 1 shows the specific arrangement of the different devices, which consists of a sand tank, an electric servo actuator, a PVC pile, two LVDTs, additional mass and steel support structures. The displacement transducers were arranged along the loading direction on both sides of the pile, placed 50 mm and 183 mm above the sand surface respectively. One side of the pile was connected to the electric servo actuator by a steel wire. The level is used to ensure that the loading point is at the same height as the connecting position of the electric servo actuator. According to Cuéllar [12] and Carswell [17], the equivalent lever arm is ~30 m in length for wind turbines of the MW-class located in the North Sea. This is corresponding to 300 mm by a scaling factor of 1:100. Based on the study of Frick and Achmus [18], the equivalent lever arm has no significant influence on the displacement accumulation for a given load magnitude. Given the available conditions in the laboratory, we chose 255 mm in the model tests. For a typical 5 MW wind turbine [19], the RNA mass is about 300,000 kg, the overall tower mass is about 350,000 kg. According to the scaling law, the total mass for the model test is nearly 0.65 kg. The additional steel ring mass which is used to connect the electric servo actuator in the model test is 0.157 kg (Fig. 1). Therefore, an additional mass of 0.5 kg was placed on top of the model pile to simulate the mass of the superstructure.

1.4. Test programme

The experimental programme was designed to study the accumulated rotation due to cyclic loadings of constant or multiple amplitude, targeting at the effect of typhoon events. Three loading patterns were considered in the tests: (1) monotonic loading, (2) continuous constant amplitude loading, and (3) multi-amplitude cyclic loading. The details of test series are presented in Table 3. First, monotonic loading tests (ST1 and ST2) were performed to determine the ultimate bearing capacity of the pile, which was used as a reference value for choice of the load magnitudes in the cyclic loading tests. However, in reality, it is impossible to identify a distinct failure point from the load-displacement curve, and there are few guidelines for proper pile failure in terms of the design criteria [8,11]. Deformation tolerances are always clarified by wind turbine manufacturers [20]. Abadie et al. [11], LebLanc et al. [8], and Byrne et al. [21] proposed that the load corresponding to a pile displacement of 0.1D at the mudline can be regarded as the ultimate bearing capacity of the pile. This criterion was applied to the tests in this paper. During the monotonic tests, the pile was gradually loaded using a servo actuator. Initially, a load of 10 N was applied to the pile at each stage in an interval of 3 min. When the load increased to 60 N, the load increment would rise to 15 N, and the loading interval still remained at 3 min. When the pile displacement at the mudline exceeded 0.1D, the loading would stop. The load schedule for monotonic tests is shown in Fig. 2.

For cyclic loading tests, a horizontal sinusoidal cyclic load was applied to the pile using the servo actuator. The characteristics of the cyclic load are defined by the following two cyclic load ratios:

$$\xi_b = F_{\max}/F_{\mathrm{u}} \tag{1}$$

$$\xi_c = F_{\min}/F_{\max} \tag{2}$$

where $F_{\max}$ and $F_{\min}$ are the maximum and minimum amplitude of the cyclic loading, F_u is the horizontal ultimate bearing capacity of the pile under static conditions ξ_b represents the magnitude of the load, and ξ_c describes the type of cyclic loading.

In this study, dynamic load is simplified as regular cyclic load with specific amplitude and frequency. By varying amplitude and number of cycles the characteristics of dynamic load are approximately represented. This simplification has often been used in model tests [8,11,12,18]. The cyclic loading tests carried out in the laboratory are limited to one-way loading, i.e. $\xi_c \geq 0$ [11]. According to LeBlanc et al. [8], the expected worst transient load is about 73 % of the ultimate bearing capacity and the fatigue load is about 30 % of

Table 2
Properties of the sand used in model tests.

Physical parameter	Value
Maximum density $\rho_{d,max}$ (g/cm^3)	1.75
Minimum density $\rho_{d,min}$ (g/cm^3)	1.43
Relative density D_r (%)	58
Average particle size d_{50} (mm)	0.55
Coefficient of nonuniformity C_u	1.97
Coefficient of curvature C_c	0.90

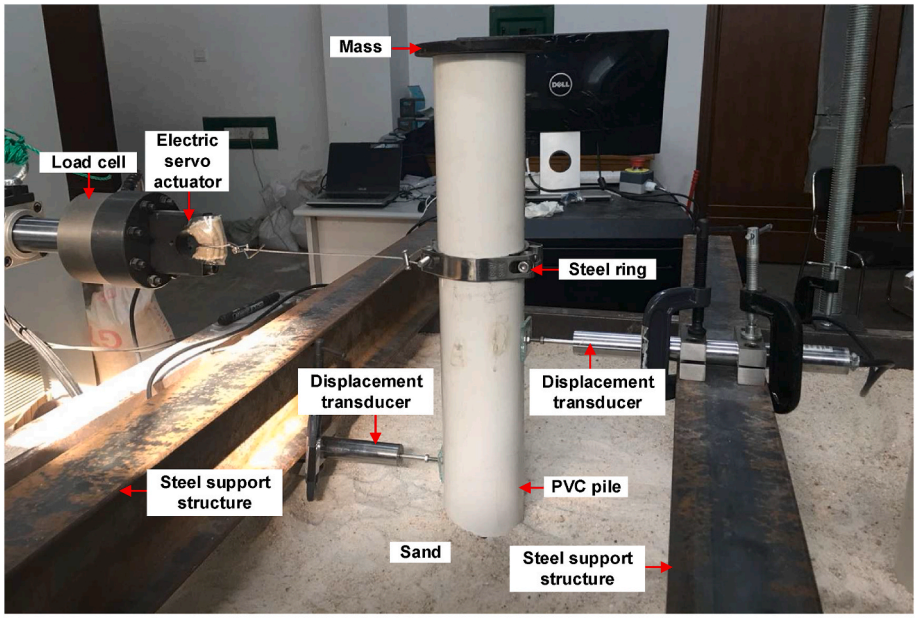

(a)

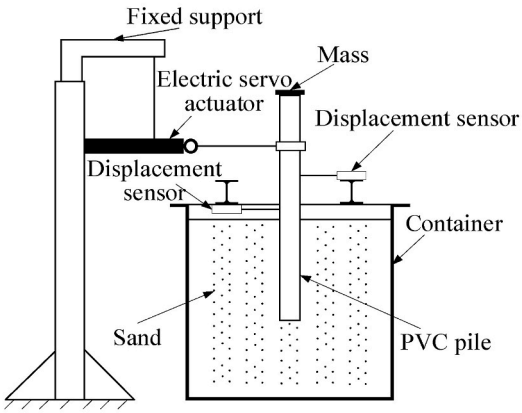

(b)

Fig. 1. Test setup: (a) Picture of test setup with the installed devices; (b) Sketch of testing rig and the loading actuator.

the ultimate bearing capacity. Therefore, the value of ξ_b for the small-amplitude cyclic load in the tests was set at about 0.3, and for comparison, two values of 0.2 and 0.4 were also adopted in the tests; the value of ξ_b for the typhoon load was set as 0.7. The frequency of wave load is higher than that of wind load and is closer to the natural frequency of offshore wind turbine. In this regard, the wave load frequency is more critical and is used in the 1-g model tests [11,12,18], and is adopted in this study. The frequency of the wave load was about 0.1 Hz [22]; according to the scaling law, the frequency of each cyclic load in the tests was set to 1 Hz. This paper focuses on the worst expected transient loads caused by the super typhoon with the highest wind speed. In China, this typhoon often appeared in the coastal areas of Fujian Province. Zhang et al. [23] collected typhoon statistics data for the past 50 years from 1961 to 2012, which showed that three super typhoons had attacked Fujian Province. The service time of offshore wind turbines is 20–25 years, so only one or two typhoon loading processes were established under typhoon conditions in the tests. Referring to the number of loading cycles with large amplitudes in the cyclic loading tests with multiple amplitudes carried out by Abadie et al. [11], the number of loading cycles of typhoon in the tests was taken as 12. As shown in Table 3, the tests CT1, CT4 and Ct7 were designed to study the accumulation rotation under constant cyclic loading with different small magnitudes, while the tests CT2, CT5, and CT8 were designed

Table 3
Summary of test conditions.

Loading mode	Test condition	Load sequence	
Static	ST1 ST2	Loading gradually until pile displacement at the mudline equaling 0.1D	
Cyclic	CT1	Without typhoon	10,000 cycles with $\xi_b = 0.2$
	CT2	With typhoon	12 cycles with $\xi_b = 0.7$ → 10,000 cycles with $\xi_b = 0.2$
	CT3	With typhoon	5000 cycles with $\xi_b = 0.2$ → 12 cycles with $\xi_b = 0.7$ → 5000 cycles with $\xi_b = 0.2$ → 12 cycles with $\xi_b = 0.7$ → 1000 cycles with $\xi_b = 0.2$
	CT4	Without typhoon	10,000 cycles with $\xi_b = 0.3$
	CT5	With typhoon	12 cycles with $\xi_b = 0.7$ → 10,000 cycles with $\xi_b = 0.3$
	CT6	With typhoon	5000 cycles with $\xi_b = 0.3$ → 12 cycles with $\xi_b = 0.7$ → 5000 cycles with $\xi_b = 0.3$ → 12 cycles with $\xi_b = 0.7$ → 1000 cycles with $\xi_b = 0.3$
	CT7	Without typhoon	10,000 cycles with $\xi_b = 0.4$
	CT8	With typhoon	12 cycles with $\xi_b = 0.7$ → 10,000 cycles with $\xi_b = 0.4$
	CT9	With typhoon	5000 cycles with $\xi_b = 0.4$ → 12 cycles with $\xi_b = 0.7$ → 5000 cycles with $\xi_b = 0.4$ → 12 cycles with $\xi_b = 0.7$ → 1000 cycles with $\xi_b = 0.4$

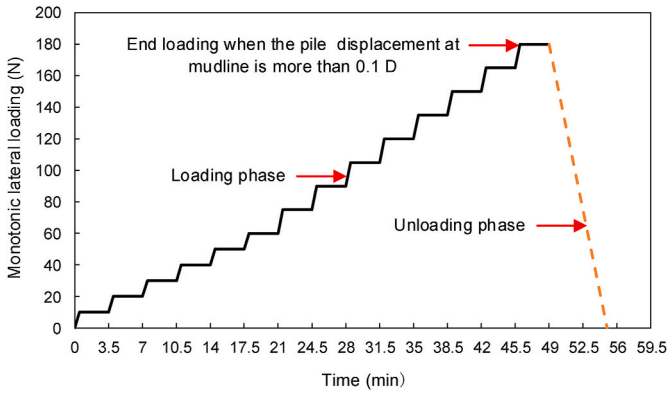

Fig. 2. Load schedule for ST1 and ST2.

to investigate the effect of a typhoon event combined with the cyclic load of small constant magnitude on the accumulated rotation of the pile. Furthermore, in order to investigate the effect of loading sequence and the number of typhoons on the accumulated rotation, model tests CT3, CT6 and CT9 were performed.

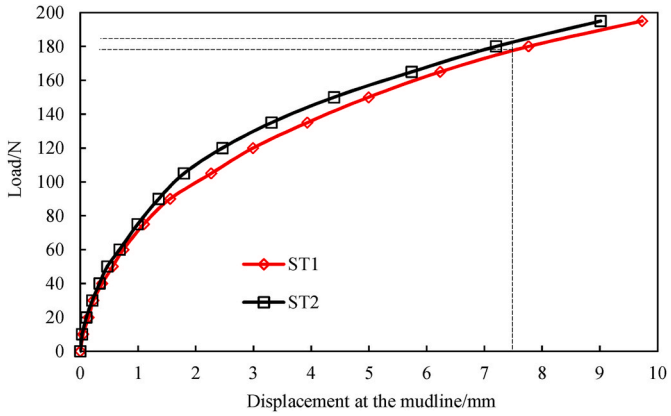

Fig. 3. Load-displacement curves at the mudline for ST1 and ST2.

2. Test results and analysis

2.1. Horizontal static loading tests

The results of the static load-displacement curves at mudline for ST1 and ST2 are shown in Fig. 3. As previously observed [8,11,12], the test results perfectly coincide with a power law. The slight differences observed between ST1 and ST2 may be caused by the inconsistency of smaller sample densities. Fig. 3 displays that for the displacement at mudline of up to 0.1D, the ultimate bearing capacity of ST1 and ST2 was 177.5 and 182.5 N, respectively. The average of the two values was taken as the ultimate bearing capacity ($F_u = 180\ N$) of the pile in all tests.

2.2. Horizontal cyclic loading tests without typhoon loads

There were three typhoon-free conditions, namely CT1, CT4 and CT7 (with similar loading sequence). The relationship between the accumulated rotation of the pile and the number of loading cycles for these three conditions in log-log axes is shown in Fig. 4. It can be seen that the accumulated rotation of the several initial cycles increases rapidly, and the growth rate decreases around the 6th cycle, and then the accumulated rotation develops with a linear growth trend until the end of the test. The second phase seems to be very consistent with the power law relationship between the accumulated rotation and the number of loading cycles. A similar trend was observed in small-scale experiments presented by LeBlanc et al. [8], Cuéllar [12] and Abadie et al. [11].

In addition, the accumulated rotation also increases with increasing ξ_b (Fig. 4). By fitting the data from the straight line starting from the 6th cycle in Fig. 4, the accumulated rotation due to the cyclic loading can be predicted by:

$$\theta_N = \beta N^{\alpha} \tag{3}$$

where θ_N is the accumulated rotation in the Nth cycle, β and α are the fitting parameters that depend on ξ_b, as shown in Table 4, and N is the number of loading cycles.

LeBlanc et al. [8] proposed a similar formula for the accumulation rotation of pile due to cyclic loading, as follows:

$$\frac{\theta_N - \theta_0}{\theta_s} = T_b(\xi_b, R_d) T_c(\xi_c) \cdot N^{0.31} \tag{4}$$

where θ_N is the accumulated rotation in the Nth cycle, θ_0 is the rotation in the first cycle, T_b and T_c are dimensionless functions that depend on the load characteristics, R_d is the relative density of the soil, and θ_s is the pile rotation in the horizontal static loading test when the load equals the maximum amplitude of the cyclic load.

A constant power coefficient of 0.31 was used to fit all curves for different ξ_b in the study of LeBlanc et al. [8]. However, the slope of the straight line under different conditions was not the same in their tests, and in some cases obvious differences can be observed. As a result, it may not be suitable to use a uniform coefficient for all conditions. Nicolai and Ibsen [24] also investigated the accumulated rotation of a stiff pile under cyclic lateral loading through small scale tests under the 1-g conditions, and found that the power coefficient in Eq. (3) is dependent on the relative density of the sand. Therefore, in this study the relationship between θ_N and the number of loading cycles is established directly. There was no static component, and a variable coefficient was used to accurately fit each curve. Fitting parameters for each condition were obtained from model tests.

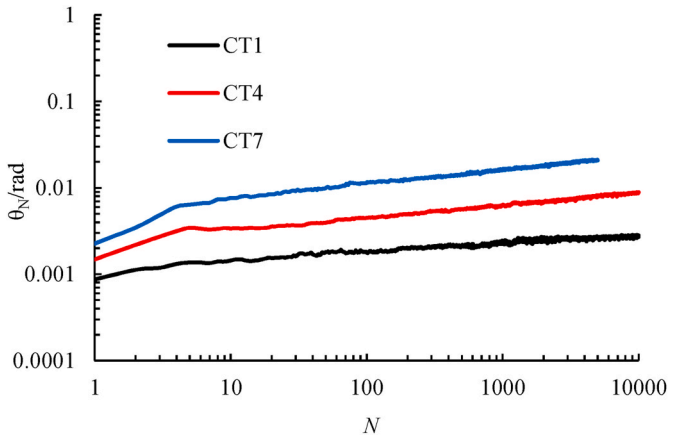

Fig. 4. Accumulated rotation against number of load cycles in log-log scale (CT1, CT, CT7).

Table 4
Fitting parameters of accumulated rotation for condition CT1, CT4 and CT7.

Condition	β	α	R^2
CT1	0.0013	0.0833	0.9098
CT4	0.0022	0.1492	0.9891
CT7	0.0051	0.1667	0.9867

Note:$R^2$is the coefficient of determination.

2.3. Horizontal cyclic loading tests with typhoon loads

Six typhoon conditions were considered in the model tests, namely CT2, CT3, CT5, CT6, CT8 and CT9. As summarized in Table 3, CT2, CT5 and CT8 each consists of 12 typhoon loading cycles at the initial stage of the loading process, while CT3, CT6 and CT9 each consists of 12 typhoon loading cycles at a later stage of the loading process. The evolution of pile accumulated rotation of CT2, CT5 and CT8 is shown in Fig. 5. It can be seen that after 12 loading cycles of typhoon, the accumulated rotation increases to a rather high value, and then there is a small decrease in the rotation for a short time under small-amplitude cyclic loads; at that point, the accumulated rotation continues to rise slowly. The growth rate of the accumulated rotation after the first 12 typhoon loading cycles is positively correlated with ξ_b.

The evolution of pile accumulated rotation of CT3, CT6 and CT9 is shown in Fig. 6. It can be seen that: 1) with the increase of ξ_b belonging to small-amplitude cyclic loads, the rotation caused by typhoon load increases sharply and decreases. This situation can be explained by the fact that a larger cyclic load can exert a stronger compressive force on the soil, which will make the soil denser, and then the lateral stiffness of the pile will become greater. Therefore, pile rotation will be smaller under the same typhoon load; 2) the sharp rise in rotation caused by the second round typhoon load is obviously smaller than that caused by the first round typhoon load. In addition, it was calculated that the second sharp rise in the rotation of CT3, CT6 and CT9 was 27.9 %, 36.4 %, and 55.9 % of the first sharp rise. Obviously, this proportion is rising, indicating that as the small-amplitude cyclic load increases, the gap between the two sharp rises in rotation caused by the typhoon load becomes smaller and smaller; 3) the growth rate of the three-stage formula divided by two rounds of typhoon load also increases with the increase of ξ_b belonging to small-amplitude cyclic loads. After two rounds of typhoon loads, the rotation of CT3 and CT6 remained almost unchanged, like a platform. However, the growth rate of CT9 is still very small, indicating that when the small-amplitude cyclic load is large, it can still increase the rotation of the pile even after two rounds of typhoon loads.

For the reason that the typhoon load has only a small number of loading cycles, the fitting parameters can only be obtained through 12 typhoon loading cycles at the beginning of the three conditions of CT2, CT5 and CT8. The previous fitting of the accumulated rotation without typhoon loads started from the 6th cycle, so the fitting of the typhoon load still started from this position. The fitting curves of these three conditions are shown in Fig. 7. It can be seen that the fitting curves of CT2 and CT8 almost coincide, while the fitting curves of CT5 are obviously staggered. Therefore, the test data of CT2 and CT8 are selected to calculate the fitting parameters of Eq. (3) for the typhoon condition. The results are shown in Table 5.

According to the fitting parameters of CT1, CT2, CT3 (Table 4) and typhoon conditions (CT2 and CT8, Table 5), α and β can be approximately predicted by

$$\beta = 0.0247{\xi_b}^{1.8665} \tag{5}$$

$$\alpha = 0.3342{\xi_b}^{0.7924} \tag{6}$$

Predictions obtained with Eqs. (5) and (6) are shown in Fig. 8(a) and (b) The correlations between β and ξ_b and between α and ξ_b are quite strong, with the R^2 as large as 0.98 and 0.93, respectively. This implies that the model can well predict α and β in Eq. (3) with ξ_b ($0 < \xi_b < 1$).

2.4. The effect of loading sequence on accumulated rotation

According to the Miner's rule, the fatigue damage of the material is approximately independent of the loading sequence [25], and the strain accumulation of the soil can be interpreted as the damage of the material [26]. LeBlanc et al. [8], Abadie et al. [11] and Barari et al. [9] found that Miner's rule provides a reasonable approximation for the prediction of the accumulated rotation under load series of varying amplitudes. Stewart [27] studied the permanent accumulated strain of the soil under cyclic loading through a triaxial test and found that its accumulated strain was independent of the loading sequence. A similar situation was also found in the tests in this article. As shown in Fig. 9, the amplitudes and cyclic number of typhoon conditions (CT5, CT6) are the same, but the loading sequence is different. For test CT5, 12 typhoon loading cycles were set at the beginning of the loading process, and then 10,000 small-amplitude cycles were followed. By contrast, for test CT6, 12 typhoon loading cycles were set in the middle of 10,000 small-amplitude cycles. The final accumulated rotations of tests CT5 and CT6 were 0.0211° and 0.0217°, respectively. The difference between these two conditions is only 2.8 %, indicating that the loading sequence has little effect on the total accumulated rotation.

The total accumulated rotation due to variable amplitude load sequences can be estimated with the simple model proposed by LeBlanc et al. [26], which was based on Miner's rule. This procedure is shown in Fig. 10. It is assumed that the pile has been subjected to N_a cycles of load type a, and then subjected to N_b cycles of load type b. It is assumed that the accumulated rotation caused by N_a

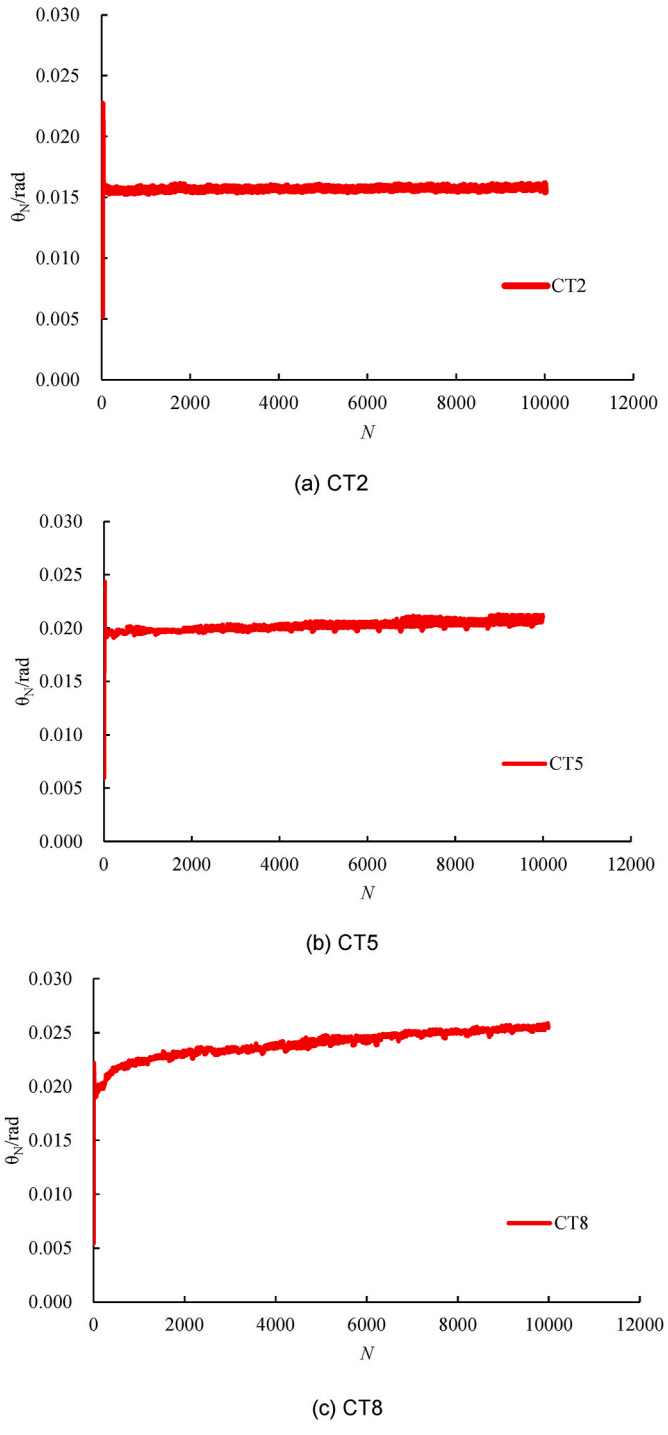

Fig. 5. Evolution of pile accumulated rotation for tests: (a) CT2, (b) CT5, (c) CT8.

cycles can be obtained equivalently by N_b^0 cycles, where N_b^0 can be referred to as the equivalent number of cycles. According to Eq. (3), the accumulated rotation caused by the cyclic load 'a' is

$$\theta_a = \beta_a (N_a)^{\alpha_a} \tag{7}$$

where α_a and β_a are the fitting parameters of the cyclic load a.

The equivalent number of cycles required for the accumulated rotation θ_a caused by the cyclic load b is

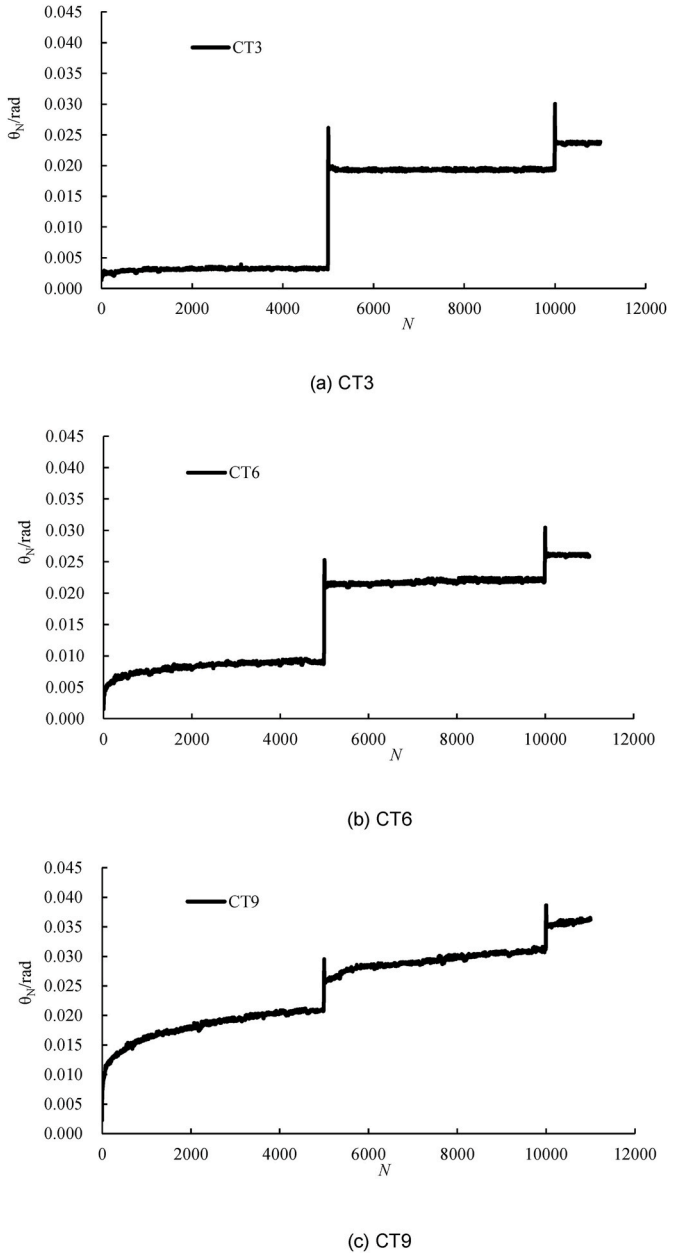

Fig. 6. Evolution of pile accumulated rotation for tests: (a) CT3, (b) CT6, (c) CT9.

$$N_b^0 = \left(\frac{\theta_a}{\beta_b}\right)^{1/\alpha_b} \tag{8}$$

where α_b and β_b are the fitting parameters of the cyclic load b.

Therefore, the overall accumulated rotation of the pile after cyclic loads a and b is given by:

$$\theta_{N_a+N_b} = \beta_b\left(N_b^0 + N_b\right)^{\alpha_b} \tag{9}$$

3. Procedures to calculate accumulated rotation during the service life

Based on Miner's linear cumulative damage rule, the accumulated rotation method of the pile caused by two magnitudes of cyclic load sequences is proposed. However, in practice, due to environmental (wave and wind) loading, the monopile foundation of offshore wind turbines will be subjected to dynamic loadings, which include many different magnitudes of cyclic loads. Therefore, to calculate

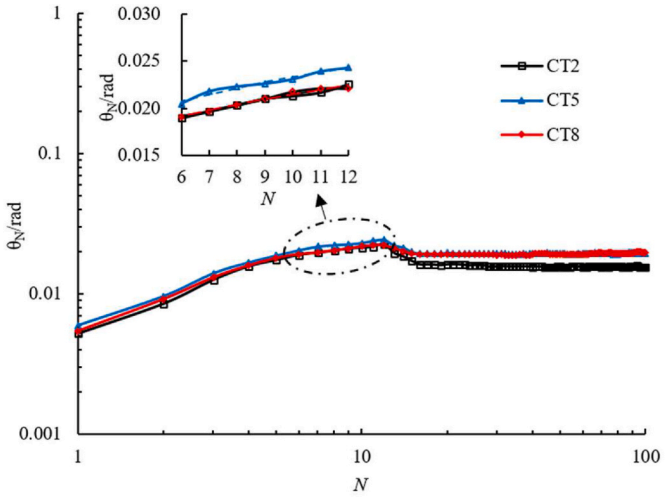

Fig. 7. Fitting curves of typhoon loads from 6th to 12th load cycle of condition CT2、CT5 and CT8.

Table 5
Fitting parameters of typhoon loads of condition CT2 and CT8.

Condition	β	α	R^2
CT2	0.0124	0.2391	0.9878
CT8	0.0126	0.2331	0.9778
Average	0.0125	0.2361	–

Note: R^2 is the coefficient of determination.

the pile accumulated rotation during its service life, all load conditions should be considered. As mentioned earlier, the loading sequence has little effect on the final accumulated rotation and can be ignored. Therefore, different types of cyclic loads can be arranged from large to small according to their amplitudes, so the typhoon loads were set at the beginning of the entire loading sequence to calculate the accumulated rotation caused by environmental loads. The procedure for estimating the total accumulated rotation during the service life is shown in Fig. 11.

4. Case study

4.1. Wind turbine and environmental conditions

Noting that wind turbines with a larger capacity (e.g. Wind Europe, 2019) have been installed in recent years [28], and in view of the adequate amount of turbines and marine meteorological data publicly available, a monopile supported GE's Haliade 6 MW wind turbine located in the northern North Sea is employed in this study [29]. The key design parameters of the reference wind turbine are presented in Table 6. The monopile has an external diameter of 7.5 m and a constant wall thickness of 0.09 m. Its embedded depth is 37.5 m for a water depth of 30 m. The tower has a total length of 85.0 m, with an outer top diameter of 4.8 m and an outer base diameter of 7.5 m, and is connected with a monopile through a transition piece. The tower base begins at the location of 15 m above the mean sea level (MSL). For simplicity, the monopile is embedded in medium dense homogeneous sand, and its properties are consistent with the sand used in the model test in this paper.

The mean wind speed at turbine hub height, ranging from 2 m/s to 66 m/s, is grouped into bins of 2 m/s [30,31]. The wind speed at a height of 10 m from the still water lever (SWL) can be calculated using the logarithmic wind shear law [32,33]:

$$V_{W,10} = V_{W,hub}\frac{\ln\left(\frac{z}{z_0}\right)}{\ln\left(\frac{z_{hub}}{z_0}\right)} \tag{10}$$

where $V_{W,\,hub}$ is the mean wind speed at the turbine hub height, $V_{W,10}$ is the mean wind speed at the height z, z_0 is the surface roughness length, which is 0.05 m for offshore according to DNV [33], z is the height above the SWL, and z_{hub} is the hub height above the SWL. The probability of occurrence of each wind speed bin is calculated by the cumulative probability distribution of the 1-h mean wind speed for northern North Sea, which is described by the 2-parameter Weibull distribution [34]:

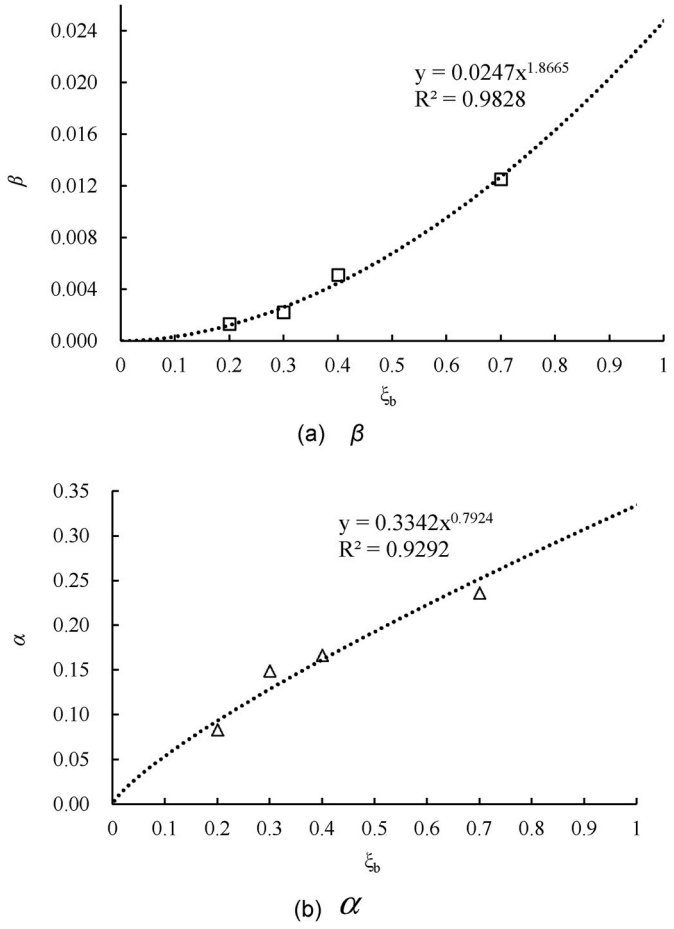

Fig. 8. Functions relating: (a) **β** and (b) **α** to ξ_b.

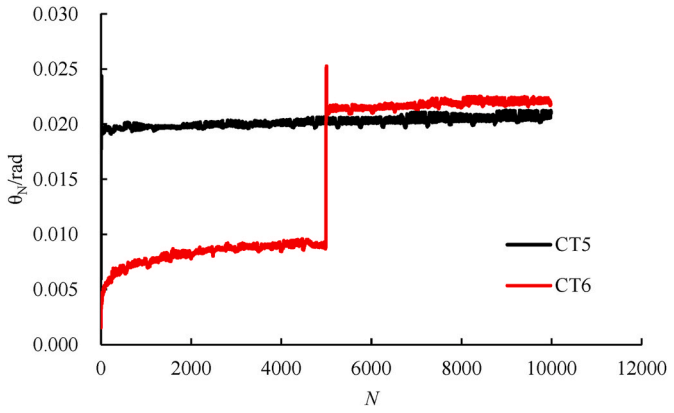

Fig. 9. Comparison of accumulated rotation of load sequence CT5 and CT6.

$$F(V_{W,10}) = 1 - \exp\left(-\left(\frac{V_{W,10}}{\beta_1}\right)^{\alpha_1}\right) \tag{11}$$

where α_1 and β_1 are the shape and scale parameters, respectively. The values $\alpha_1 = 1.708$ and $\beta_1 = 8.426$ were determined based on measurements from the northern North Sea during the 1973–99 period [34]. Corresponding to the Mead wind speed $V_{W,10}$, the effective wave height and peak period are estimated by Eqs. (12) and (13), respectively, as proposed by Johannessen et al. [34]:

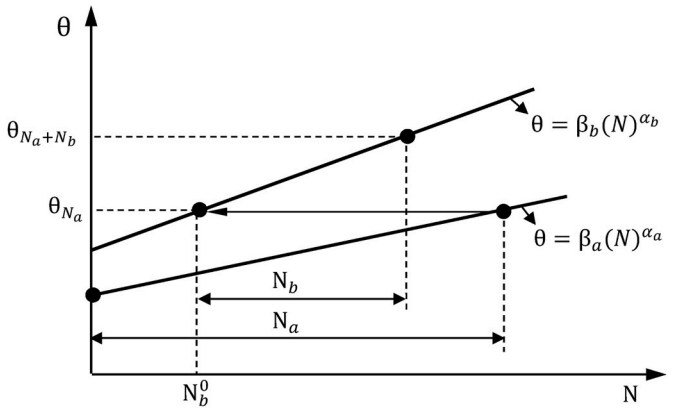

Fig. 10. Calculating accumulated rotation of the pile under different cyclic loads with superposition method.

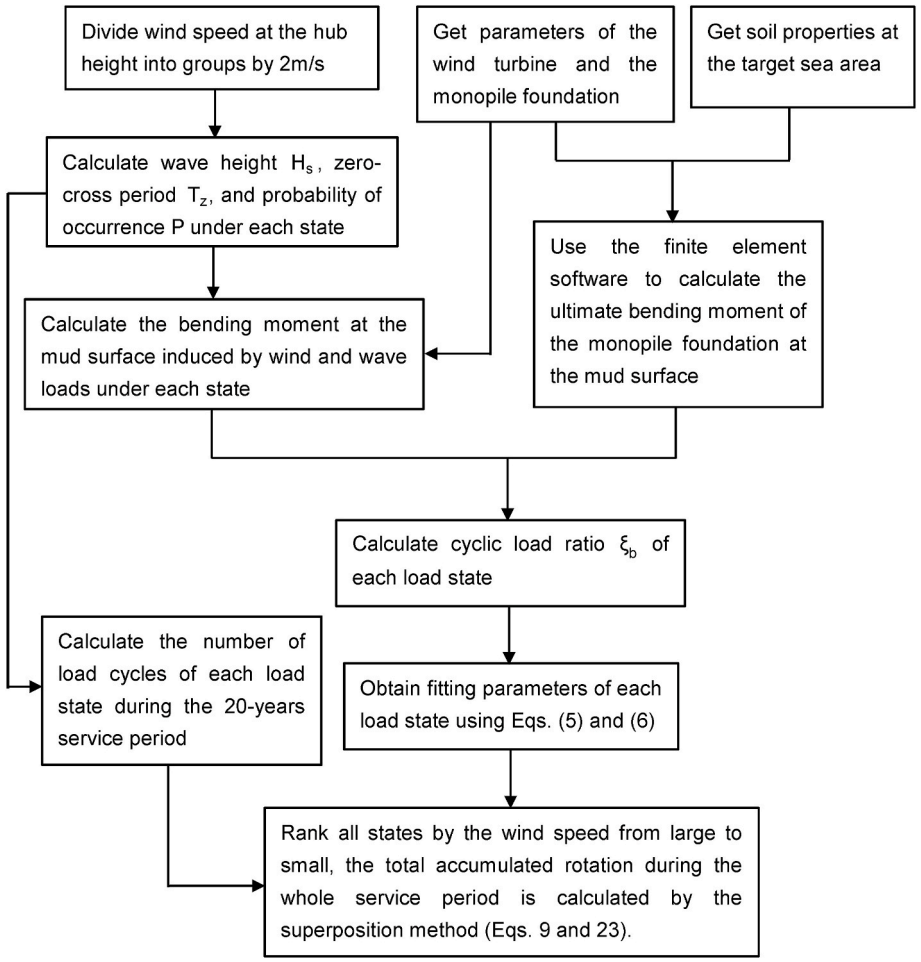

Fig. 11. Procedures of estimating the accumulated rotation.

$$H_s = \left(\frac{V_{W,10} - 1.764}{3.426}\right)^{\frac{1}{0.78}} \tag{12}$$

$$T_P = 4.883 + 2.68 \times H_S^{0.529} \tag{13}$$

Table 6
Parameters of Haliade 6 MW wind turbine.

Parameter	Value
Cut-in wind speed (m/s)	3
Cut-out wind speed (m/s)	25
Rated wind speed (m/s)	12
Number of blades	3
Length of blade (m)	73.5
Chord length, max (m)	5
Rotor diameter r (m)	151
Swept area (m^2)	17860
Hub height from MSL (m)	100

where T_P is the peak period and H_S is the significant wave height.

Finally, Hua [35] proposal based on the empirical relationship between the peak wave period and the zero-crossing period is given by Eq. (14) as follows:

$$T_Z = \frac{1}{1.41} T_P \tag{14}$$

where T_Z is the wave zero-crossing period.

Based on the above description, the probability of occurrence of a particular wave height with zero-crossing periods for varying wind speeds is summarized in Table 7, resulting in a total of 33 environmental states. It should be noted that the target of these environmental states is inclusion in all probable cases with a total probability of occurrence of 100 %.

4.2. Wind load

Wind-generated loads on the rotor and the tower will be considered. For the wind load on the rotor, two cases will be considered. The first is the rotor in operating mode, indicating that the range of the mean wind speed varies from cut-in to cut-out. The second is

Table 7
Marine meteorological data.

State	V_W(m/s)	V_{10} (m/s)	T_z(s)	H_S(m)	P_{State}
1	2	1	3.5	0.0	0.045237053
2	4	3	4.3	0.2	0.09512168
3	6	4	5.0	0.6	0.120521216
4	8	6	5.5	1.1	0.129008167
5	10	7	6.0	1.7	0.124987543
6	12	8	6.4	2.3	0.112662419
7	14	10	6.8	3.0	0.095837591
8	16	11	7.2	3.6	0.077595275
9	18	13	7.6	4.3	0.06013321
10	20	14	8.0	5.1	0.044781008
11	22	15	8.3	5.8	0.032140507
12	24	17	8.6	6.6	0.022283343
13	26	18	9.0	7.4	0.014950875
14	28	20	9.3	8.2	0.009722067
15	30	21	9.6	9.1	0.006134761
16	32	22	9.9	9.9	0.003760492
17	34	24	10.2	10.8	0.00224129
18	36	25	10.4	11.7	0.001299889
19	38	26	10.7	12.6	0.000734139
20	40	28	11.0	13.5	0.000404007
21	42	29	11.3	14.5	0.000216764
22	44	31	11.5	15.4	0.000113448
23	46	32	11.8	16.4	5.79462E-05
24	48	33	12.1	17.3	2.88975E-05
25	50	35	12.3	18.3	1.40759E-05
26	52	36	12.6	19.3	6.69934E-06
27	54	38	12.8	20.3	3.1166E-06
28	56	39	13.1	21.3	1.41763E-06
29	58	40	13.3	22.4	6.30682E-07
30	60	42	13.5	23.4	2.74502E-07
31	62	43	13.8	24.4	1.16919E-07
32	64	45	14.0	25.5	4.8746E-08
33	66	46	14.2	26.6	1.98982E-08

that the rotor stops completely and the wind directly acts on the blades of the rotor, indicating that the mean wind speed is less than the value of cut-in or more than the cut-out. The thrust force (F_{th}) on the rotor during operation mode can be simply calculated as follows [22,36]:

$$F_{th} = \frac{1}{2}\rho_a A_R C_T V_{W,hub}^2 \tag{15}$$

where F_{th} is the thrust force on the rotor, $\rho_a = 1.225\ \ \mathrm{kg/m^3}$ is the density of air, $A_R = 17860\ \mathrm{m^2}$ is the swept area of the blades, and C_T is the thrust coefficient:

1) When the wind speed fluctuates between the value of cut-in and the rated speed, the thrust coefficient can be calculated using the formula proposed by Frohboese and Schmuck [37]:

$$C_T = \frac{3.5\left(2V_{W,hub} - 3.5\right)}{V_{W,hub}^2} \approx \frac{7}{V_{W,hub}} \tag{16}$$

The thrust coefficient should not exceed 1 [22].

2) When the wind speed fluctuates between the value of cut-out and the rated speed V_R, it is assumed that the power remains stable, thus the thrust coefficient is expressed as [22]:

$$C_T = 3.5V_R(2V_R + 3.5)\cdot\frac{1}{V_{W,hub}^3} \approx 7\cdot\frac{V_R^2}{V_{W,hub}^3} \tag{17}$$

3) When the wind speed is less than the value of cut-in or greater than the cut-out speed, the blades will stop rotating, and the thrust force T_h [38] on the blades is calculated using the following formula:

$$T_h = \frac{1}{2}\rho_a A_B C_T V_{W,hub}^2 \tag{18}$$

where A_B is the projected area of three blades, and the maximum chord length of the turbine is 5 m, so the projected area of the individual blade is 183.75 $\mathrm{m^2}$, and B is the number of blades, which is 3 here. When the wind speed is greater than the cut-out speed, the thrust coefficient is 1.7 [38]. When the wind speed is less than the cut-in speed, the thrust coefficient is taken as 1.

The wind load acting on the turbine tower depends on the wind velocity along the tower. The tower is evenly divided into five segments and the wind load is treated as a concentrated load in each segment. The wind load is calculated as follows [39]:

$$F_{tower}^{Z_i} = 0.5\rho_a C_s A_{tower}^{z_i} V_{z_i}^2 \tag{19}$$

where $F_{tower}^{Z_i}$ is the wind load acting at height z_i in N; $A_{tower}^{z_i}$ is the wind pressure area at height z_i in $\mathrm{m^2}$; C_s is the shape coefficient which equals 0.5 for the tubular steel tower; z_i is the height above the sea water level of the segment i. The wind profile V_{z_i}, denotes the average wind speed as a function of the height z_i. In the case of standard wind turbines, the normal wind speed profile is given by the power law [39]:

$$V_{z_i} = V_{w,hub}\left(\frac{z_i}{z_{hub}}\right)^{\alpha} \tag{20}$$

where z_{hub} is the height of the hub; α is the power law exponent which is assumed to be 0.2. Combing these parameters, the thrust force on the blades in each state can be calculated using Eqs. (15) and (18), and using the water depth h_w and hub height above mean sea level H_{hub}.

The bending moment at mudline arising from the wind is estimated as

$$M_{wind} = T_h(h_w + H_{hub}) + \sum_{i=1}^{5} F_{tower}^{Z_i} \times (z_i + 30) \tag{21}$$

Compared with the bending moment caused by the thrust and wave loads, the bending moment caused by the overhand of RNA is minor and therefore is not included in Eq. (21).

4.3. Wave load

The wave load on a monopile can be predicted by the Morison equation, which consists of inertia and drag components. For the structural configuration considered here, the inertia component of the wave loading is dominant compared to the drag component [40]. Tempel [32] deduced the bending moment at the mudline generated by the wave load as follows:

$$M_{wave} = \rho_{water} g \frac{C_M \pi D^2}{4} \zeta d \left[\tanh(k_{wave} d) + \frac{1}{k_{wave} d} \left(\frac{1}{\cosh(k_{wave} d)} - 1 \right) \right] \tag{22}$$

where M_{wave} is the bending moment at the mudline generated by the wave force, ρ_{water} is the density of water, which is 1000 kg/m^3, D is the external diameter of the pile, d is the water depth, k_{wave} is the wave number, $k_{wave} = 4\pi^2/(gT_S^2)$, ζ is the wave amplitude, $\zeta = H_s/2$, C_M is the inertial force coefficient (2 for a smooth tubular section) [33], and g is the gravitational acceleration.

4.4. α and β for all environmental states

According to the above method, the bending moments at the mudline caused by wind and wave loadings, which correspond to the 33 environmental conditions, are presented in Table 8. The horizontal ultimate bearing capacity is determined by a finite element (ABAQUS) static pushover analysis at a moment arm of 25.5 m, which has been used in Ma's previous studies [7,36]. The parameters used in the finite element model are typical for medium dense sand in the North Sea and are listed in Table 9. The steel monopile material is assumed to be linearly elastic, with a Young's modulus of 210 GPa, a Poisson's ratio of 0.3, and a density of 7850 kg/m^3. The ultimate bearing capacity corresponding to the 0.1D displacement at the mudline is 1266.8 MN m. The cyclic load ratio ξ_b for each state is obtained by dividing the ultimate bearing capacity by the bending moments at the mudline, then β and $\boldsymbol{\alpha}$ are calculated according to Eqs. (5) and (6), respectively. Considering the cyclic load frequency value of 0.1 Hz, the wind turbine will be subject to 6×10^7 loading cycles during a service life of 20 years, and the corresponding number of loading cycles will be calculated according to the probability of occurrence of each state in Table 7. Following the procedure for estimating the total accumulated rotation during the service life, as shown in Fig. 11, the total accumulated rotation can be calculated by iterations as follows:

$$\begin{aligned} &\theta_i^T = \beta_i (N_i)^{\alpha_i} \\ &N_{i-1}^{i,eq} = \left(\frac{\theta_i^T}{\beta_{i-1}} \right)^{\alpha_{i-1}} \\ &\theta_{i-1}^T = \beta_{i-1} \left(N_{i-1}^{i,eq} + N_{i-1} \right)^{\alpha_{i-1}} \\ &for\ i = 33, 32, \ldots, 2 \end{aligned} \tag{23}$$

where i is the serial number of the load state, from 33 to 2, θ_i^T is the total accumulated rotation to *ith* load state, θ_{i-1}^T is the total accumulated rotation to $(i-1)th$ load state, N_i is the number of load cycles of *ith* load state, $N_{i-1}^{i,eq}$ is the equivalent number of load cycles (Eq. (8)), β_i and α_i are parameters, which are calculated by Eqs. (5) and (6) respectively. The calculation results are summarized in Table 10.

4.5. Results and discussion

According to the Grade of Tropical Cyclones (GB/T19201-2006) [41], when the wind speed at 10 m above sea level is greater than 32.7 m/s, the tropical cyclone reaches the typhoon level, so the states of 24–33 listed in Table 8 are considered as typhoon conditions. As explained above, the loading sequence has little effect on the final accumulated rotation. Therefore, the states in Table 8 are ranked from large to small according to the wind speed. As shown in Table 10, typhoon conditions are arranged at the beginning of the entire loading process, and the final accumulated rotation under this load sequence can be approximately considered equal to the final accumulated rotation under any other possible load sequences. Based on the above assumption, the final accumulated rotation induced by cyclic loading during the 20-year service period of the wind turbine was calculated according to Miner's rule, and the results are presented in Table 10. It can be seen that the final accumulated rotation under all load states during the service period is 0.27753°, which is a value that close to the tolerance criterion (0.25°, DNV. GL). The accumulated rotation induced by the typhoon load corresponding to typhoon states (24–33) was 0.27752°, hence the accumulated rotation induced by the typhoon load accounts for almost 100 % of the final accumulated rotation.

LeBlanc et al. [26] proposed a method for estimating the accumulated rotation of a stiff pile in sand during the storm, and the validity of the method was checked using by a series of 1-g model tests. An example of 2 MW turbine was also given to illustrate how to use this method. In their study, the load conditions were divided into the ultimate, serviceability and fatigue limit states during the lifetime. The results showed that the ULS load contributes 68 % of the total accumulated rotation. Similar results were observed in this study that the cyclic load during a typhoon event has a much larger influence than the small cyclic load with more cycle numbers. Recently, Wang and Larsen [5] presented a workflow to predict the permanent accumulated rotation of a monopile in sand during an extreme storm event using the method in Ref. [26] and considered the effect of fully nonlinear irregular waves; the results confirmed the importance of the extremely large load cycles associated with the storm and also indicated that the nonlinear irregular waves have

Table 8
Relevant parameters of cyclic loads for all states.

State	M_{tower} (MNm)	M_{th} (MNm)	M_{wave} (MNm)	M_{total} (MNm)	ξ_b	N	β	α
1	0	0.2	0	0.21	0.000	2714223	2.16137E-09	0.000337
2	0.1	22.8	1.9	24.79	0.020	5707301	1.59901E-05	0.014799
3	0.3	51.2	6.6	58.10	0.046	7231273	7.83921E-05	0.029062
4	0.5	79.6	11.3	91.39	0.072	7740490	0.000182615	0.041615
5	0.7	99.5	16.0	116.30	0.092	7499253	0.000286346	0.050371
6	1.1	119.5	20.7	141.25	0.112	6759745	0.000411595	0.05876
7	1.4	102.4	25.4	129.22	0.102	5750255	0.000348563	0.054756
8	1.9	89.6	29.9	121.41	0.096	4655717	0.00031029	0.052118
9	2.4	79.6	34.3	116.38	0.092	3607993	0.000286693	0.050397
10	3.0	71.7	38.6	113.25	0.089	2686860	0.000272476	0.049321
11	3.6	65.2	42.7	111.46	0.088	1928430	0.000264497	0.048702
12	4.3	59.7	46.7	110.65	0.087	1337001	0.00026092	0.048422
13	5.0	50.4	50.4	105.86	0.084	897052	0.000240272	0.046756
14	5.8	58.5	54.0	118.30	0.093	583324	0.000295631	0.051058
15	6.7	67.2	57.4	131.21	0.104	368086	0.000358665	0.055425
16	7.6	76.4	60.6	144.60	0.114	225630	0.000430025	0.059863
17	8.5	86.3	63.7	158.48	0.125	134477	0.000510169	0.064368
18	9.6	96.7	66.6	172.84	0.136	77993	0.000599859	0.068949
19	10.7	107.7	69.3	187.69	0.148	44048	0.000699651	0.073604
20	11.8	119.4	71.8	203.05	0.160	24240	0.000810319	0.078338
21	13.0	131.6	74.3	218.92	0.173	13006	0.000932532	0.083152
22	14.3	144.5	76.5	235.32	0.186	6807	0.001067063	0.088048
23	15.6	157.9	78.7	252.23	0.199	3477	0.00121463	0.093026
24	17.0	171.9	80.7	269.69	0.213	1734	0.001376253	0.098093
25	18.5	186.5	82.7	287.69	0.227	845	0.001552632	0.103245
26	20.0	201.8	84.5	306.23	0.242	402	0.001744675	0.108485
27	21.6	217.6	86.2	325.34	0.257	187	0.00195333	0.113815
28	23.2	234.0	87.8	345.01	0.272	85	0.00217947	0.119233
29	24.9	251.0	89.4	365.25	0.288	38	0.002424234	0.124744
30	26.6	268.6	90.8	386.06	0.305	16	0.002688435	0.130344
31	28.4	286.8	92.2	407.46	0.322	7	0.002973158	0.136036
32	30.3	305.6	93.5	429.44	0.339	3	0.00327953	0.141819
33	32.2	325.0	94.8	452.02	0.357	1	0.003608574	0.147694

Note: M_{tower}, M_{th} and M_{wave} are the bending moment at mudline caused by wind load on the tower, the thrust load on the rotor and the wave load, respectively.

Table 9
Soil properties used in analysis.

Type of sand	Unit weight ($kN.m^{-3}$)	Young's Modulus (MPa)	Angle of friction (deg.)	Cohesion (kPa)	Friction coefficient
Medium	10	40	34	0.5	0.45

limited influence on the permanent accumulated rotation.

The important implications of this study to the current methodologies for predicting the permanent accumulated rotation of monopile foundations of offshore wind turbines are as follows: (1) the accumulated rotation induced by small-amplitude cyclic loading can be ignored; (2) the permanent accumulated rotation of the monopole foundation over the entire design life can be expressed by the rotation induced by typhoon conditions. Then the whole process of calculating the accumulated rotation is simplified.

5. Conclusions

This paper presents the results from a series of model tests which aimed to investigate the impact of typhoons on the accumulated deformation of monopile of offshore wind turbines and a simple method for estimating the permanent accumulated rotation of monopile during turbine's lifetime. The main findings and conclusions of the study can be summarized as follows.

(1) When only one type of cyclic load is applied to the pile, the accumulated rotation of the pile under lateral cyclic loading in sand can be predicted by a power function of the number of loading cycles (Eq. (3)), and the larger cyclic load ratio ξ_b is, the larger the power coefficient will be.
(2) The larger and very few load cycles corresponding the typhoon events can cause a sharp rise in the accumulated rotation, and the total accumulated rotation is mainly caused by the typhoon load series.
(3) The loading sequence has little effect on the accumulated rotation of the monopile. Miner's rule-based superposition can provide a reasonable approximation for the permanent accumulated rotation subject to variable cyclic loadings.

Table 10
Calculation results of accumulated rotation.

State	ξ_b	θ (rad)	θ_N (rad)	θ_N (°)
33	0.357	0.003608574	0.003608574	0.206860905
32	0.339	0.000507419	0.004115992	0.235948595
31	0.322	0.000286815	0.004402807	0.252390196
30	0.305	0.000181597	0.004584403	0.262800193
29	0.288	0.00011989	0.004704294	0.269672891
28	0.272	7.10467E-05	0.004775340	0.273745630
27	0.257	3.82315E-05	0.004813572	0.275937246
26	0.242	1.78909E-05	0.004831463	0.276962838
25	0.227	7.02938E-06	0.004838492	0.277365796
24	0.213	2.2294E-06	0.004840722	0.277493596
23	0.199	5.49091E-07	0.004841271	0.277525073
22	0.186	1.00788E-07	0.004841371	0.277530850
21	0.173	1.30813E-08	0.004841385	0.277531600
20	0.160	1.13169E-09	0.004841386	0.277531665
19	0.148	6.05538E-11	0.004841386	0.277531668
18	0.136	1.82828E-12	0.004841386	0.277531669
17	0.125	2.75335E-14	0.004841386	0.277531669
16	0.114	1.77809E-16	0.004841386	0.277531669
15	0.104	0	0.004841386	0.277531669
14	0.093	0	0.004841386	0.277531669
13	0.084	0	0.004841386	0.277531669
12	0.087	0	0.004841386	0.277531669
11	0.088	0	0.004841386	0.277531669
10	0.089	0	0.004841386	0.277531669
9	0.092	0	0.004841386	0.277531669
8	0.096	0	0.004841386	0.277531669
7	0.102	0	0.004841386	0.277531669
6	0.112	0	0.004841386	0.277531669
5	0.092	0	0.004841386	0.277531669
4	0.072	0	0.004841386	0.277531669
3	0.046	0	0.004841386	0.277531669
2	0.020	0	0.004841386	0.277531669
1	0.000	0	0.004841386	0.277531669

(4) The permanent accumulated rotation of the monopile throughout the design life is mainly contributed by cyclic loading induced by typhoons while the contribution of cyclic loading with small amplitudes in the loading sequences can be ignored.

The method for estimating the accumulated rotation of the monopile are based on limited 1-g model tests and Miner's rule. Further work to validate the resulting using centrifuge tests and advanced numerical modeling is desirable. Otherwise, future work should be carried out to investigate the effect of irregular waves, dynamic loads on the accumulated rotation.

Declaration of competing interest

The authors declare that they have no known competing financial interests or personal relationships that could have appeared to influence the work reported in this paper.

Acknowledgments

The authors wish to acknowledge the financial support provided by the National Key Research and Development Program (No. 2019YFB1503700) and by the Research Grants Council of Hong Kong (C7038-20G).

Notation

The following symbols are used in this paper

A_B projected area of an individual blade
A_R sweeping area of the blades
B number of blades
C_M inertial force coefficient
C_T thrust coefficient
d water depth
D external diameter of the pile
$F_{\max}$ $F_{\min}$ maximum and minimum amplitude of the cyclic loading

F_{th}	thrust force on the rotor
F_u	horizontal ultimate bearing capacity of the pile under static conditions
g	gravitational acceleration
H_S	effective wave height
M_{wave}	bending moment at the mudline generated by the wave force
N	number of loading cycles
R_d	relative density of soil
T_b	T_c dimensionless functions depending on the load characteristics
T_h	thrust force on the blades
T_P	peak period
$V_{W,\,hub}$	mean wind speed at the turbine hub height
$V_{W,10}$	mean wind speed at height z
z	height above the SWL
z_0	surface roughness length
z_{hub}	hub height
β, α	fitting parameters
α_1	β_1 the shape and scale parameters of wind speed
R^2	coefficient of determination
ξ_b	intensity of the load
ξ_c	type of cyclic loading
θ_N	accumulated rotation in the Nth cycle
θ_0	rotation in the first cycle
θ_s	pile rotation in the horizontal static loading
ρ_a	density of air
ρ_{water}	density of water
k_{wave}	wave number
SWL	sea water level

References

[1] GWEC. Global wind report 2018. Global Wind Energy Council report; 2019.
[2] Musial W, Beiter P, Spitsen P, Nunemaker J, Gevorgian V. Offshore wind technologies market report. U.S. Department of Energy; 2018.
[3] Achmus M, Thieken K, Saathoff JE, Terceros M, Albiker J. Un- and reloading stiffness of monopile foundations in sand. Appl Ocean Res 2019;84:62–73.
[4] Schmoor KA, Achmus M. Optimum geometry of monopiles with respect to the geotechnical design. Journal of Ocean and Wind Energy 2015;2(1):54–60.
[5] Wang SF, Larsen TJ. Permanent accumulated rotation of an offshore monopile wind turbine in sand during a storm. Ocean Eng 2019;188:1–13.
[6] Sun YX. Experimental and numerical studies on a laterally loaded monopole foundation of offshore wind turbine. PhD Thesis. Zhejiang: Zhejiang University; 2017.
[7] Ma HW, Yang J, Chen LZ. Numerical analysis of the long-term performance of offshore wind turbines supported by monopiles. Ocean Eng 2017;36:94–105.
[8] LeBlanc C, Houlsby GT, Byrne BW. Response of stiff piles in sand to long-term cyclic lateral loading. Geotechnique 2010;60(2):79–90.
[9] Barari A, Bagheri M, Rouainia M, Ibsen LB. Deformation mechanisms for offshore monopole foundations accounting for cyclic mobility effects. Soil Dynam Earthq Eng 2017;97:439–53.
[10] Wilkie D, Galasso C. Site-specific ultimate limit state fragility of offshore wind turbines on monopile substructures. Eng Struct 2020;204:109903.
[11] Abadie CN, Byrne BW, Houlsby GT. Rigid pile response to cyclic lateral loading: laboratory. Geotechnique 2019;69(10):863–76.
[12] Cuéllar P. Pile foundations for offshore wind turbines: numerical and experimental investigations on the Behavior under short-term and long-term loading. PhD Thesis. Berlin: Technische Universität Berlin; 2011.
[13] Roesen HR, Ibsen LB, Andersen LV. Experimental testing of monopoles in sand subjected to one-way long-term cyclic lateral loading. In: Proceedings of the 18th international conference on soil mechanics and geotechnical engineering. Paris: Presses des Ponts; 2013. p. 2391–4.
[14] Long YQ, Bao SH. Structural mechanics. China: Higher Education Press; 1988.
[15] Wang LZ, Zhu B, Lai XH. Cyclic accumulative deformation of sand and its explicit model. Chin J Geotech Eng 2015;37(11):2024–9.
[16] GB/T50123-1999. Standard for soil test method. Beijing: China Architecture & Building Press; 2015.
[17] Carswell W. Soil-structure modeling and design considerations for offshore wind turbine monopile foundations. Ph. D Thesis, University of Massachusetts Amherst; 2015.
[18] Frick D, Achmus M. An experimental study on the parameters affecting the cyclic lateral response of monopiles for offshore wind turbines in sand. Soils Found 2020;60(6):1570–87.
[19] Jonkman J, Butterfield S, Musial W, Scott G. Definition of a 5-MW reference wind turbine for offshore system development. 2009. Technical Report NREL/TP-500-38060.
[20] DNV·GL-ST-0126. Support structures for wind turbines. Oslo, Norway: DNV; 2016.
[21] Byrne BW, MacAdam R, Burd HJ, Houlsby GT, Martin CM, Gavin K, Doherty P, Igoe D, Zdravković DNG, et al. Field testing of large diameter piles under lateral loading for offshore wind applications. In: Proceedings of the XVI ECSMGE geotechnical engineering for infrastructure and development. London, UK: ICE publishing; 2015. p. 1255–60.
[22] Arany L, Bhattacharya S, Macdonald J, Hogan SJ. Design of monopoles for offshore wind turbines in 10 steps. Soil Dynam Earthq Eng 2017;92:126–52.
[23] Zhang RY, Zhang XZ, Cai LW, Li BL. The impact of tropical cyclones on coastal wind farm development in China. Mete Rological Monthly 2009;35(12):88–95.
[24] Nicolai G, Ibsen LB. Small-scale testing of cyclic laterally loaded monopiles in dense saturated sand. In: The twenty-fourth international Ocean and polar engineering conference; 2014. ISOPE-I-14-234, Korea.
[25] Miner MA. Cumulative damage in fatigue. J Appl Mech 1945;67:159–64.
[26] LeBlanc C, Byrne BW, Houlsby GT. Response of stiff piles to random two-way lateral loading. Geotechnique 2010;60(9):715–21.
[27] Stewart HE. Permanent strains from cyclic variable amplitude loadings. Journal of Geotechnical Engineering 1986;112(6):646–60.

[28] Wind Europe. Offshore Wind in Europe - key trends and statistics 2018. February 2019. Published.
[29] GE's Haliade 150-6MW. High yield offshore wind turbine. Available at: https://www.ge.com/content/dam/ge-renew-new/downloads/brochures/wind-offshore-haliade-wind-turbine.pdf.
[30] Løken IB, Kaynia AM. Effect of foundation type and modelling on dynamic response Wind. Energy 2019:1–19.
[31] Amirinia G, Jung S. Buffeting response analysis of offshore wind turbines subjected to hurricanes. Ocean Eng 2017;141:1–11.
[32] van der Tempel J. Design of support structure for offshore wind turbines. PhD thesis. Netherland: Delf University of Technology; 2006.
[33] DNV. DNV-OS-J101. Offshore standard: design of offshore wind turbine structures. Hellerup, Denmark: Det Norske Veritas; 2014.
[34] Johannessen K, Meling TS, Stavanger SHS. Joint distribution for wind and waves in the northern North sea. Int J Offshore Polar Eng 2002;12(1):19–28.
[35] Hua F, Fan B, Lu Y, Wang JQ. An empirical relation between sea wave spectrum peak period and zero-crossing period. Adv Mar Sci 2004;22(1):16–20.
[36] Ma HW, Yang J. A novel hybrid monopile foundation for offshore wind turbines. Ocean Eng 2020;198:106963.
[37] Frohboese P, Schmuck C. Thrust coefficients used for estimation of wake effects for fatigue load calculation. Polland: Warsaw: European Wind Energy Conference; 2010. p. 1–10.
[38] Fan HY. Dynamics and fatigue analysis on monopile foundation of offshore wind t turbine under wind and wave loads. Master Thesis. China: Harbin Institute of Technology; 2016.
[39] ABS Guide for building and classing offshore wind turbine installations. American Bureau of Shipping ABS Plaza; 2010.
[40] Rezaei R. Fatigue sensitivity of monopile-supported offshore wind turbines. PhD thesis. London: University College London; 2017.
[41] GB/T19201-2006. Grade of tropical cyclones. Bei Jing: Standards Press of China; 2006.